HHS Public Access

Author manuscript

Anal Bioanal Chem. Author manuscript; available in PMC 2022 November 01.

Published in final edited form as:

Anal Bioanal Chem. 2021 November ; 413(27): 6689–6701. doi:10.1007/s00216-021-03640-w.

Biocompatible reference electrodes to enhance chronic electrochemical signal fidelity in vivo

Blake T. Seaton[1], **Michael L. Heien**[1]

[1]Department of Chemistry and Biochemistry, University of Arizona, Tucson, AZ 85721, USA

Abstract

In vivo electrochemistry is a vital tool of neuroscience that allows for the detection, identification, and quantification of neurotransmitters, their metabolites, and other important analytes. One important goal of in vivo electrochemistry is a better understanding of progressive neurological disorders (e.g., Parkinson's disease). A complete understanding of such disorders can only be achieved through a combination of acute (i.e., minutes to hours) and chronic (i.e., days or longer) experimentation. Chronic studies are more challenging because they require prolonged implantation of electrodes, which elicits an immune response, leading to glial encapsulation of the electrodes and altered electrode performance (i.e., biofouling). Biofouling leads to increased electrode impedance and reference electrode polarization, both of which diminish the selectivity and sensitivity of in vivo electrochemical measurements. The increased impedance factor has been successfully mitigated previously with the use of a counter electrode, but the challenge of reference electrode polarization remains. The commonly used Ag/AgCl reference electrode lacks the long-term potential stability in vivo required for chronic measurements. In addition, the cytotoxicity of Ag/AgCl adversely affects animal experimentation and prohibits implantation in humans, hindering translational research progress. Thus, a move toward biocompatible reference electrodes with superior chronic potential stability is necessary. Two qualifying materials, iridium oxide and boron-doped diamond, are introduced and discussed in terms of their electrochemical properties, biocompatibilities, fabrication methods, and applications. In vivo electrochemistry continues to advance toward more chronic experimentation in both animal models and humans, necessitating the utilization of biocompatible reference electrodes that should provide superior potential stability and allow for unprecedented chronic signal fidelity when used with a counter electrode for impedance mitigation.

Keywords

Reference electrodes; In vivo electrochemistry; Biofouling; Iridium oxide; Boron-doped diamond

Introduction

Understanding the brain and nervous system via electrical measurement has become an essential scientific tool since the mid-seventeenth century, when Jan Swammerdam first

✉Michael L. Heien, mheien@arizona.edu.

Conflict of interests The authors declare no competing interests.

induced the contraction of a frog leg muscle by stimulating its adherent nerve [1]. Today, there are two major methods of electrical measurement in neuroscience: electrophysiology and electrochemistry. In general, electrophysiological methods measure the synaptic and firing activity of neurons (i.e., electrical communication), whereas electrochemical methods measure the release of neurotransmitters, metabolites, and other analytes (i.e., chemical communication). Many in vivo electrochemical methods rely upon the measurement of redox reactions (e.g., voltammetry, amperometry), while others rely upon galvanostatic, impedimetric, or potentiometric measurements (e.g., potentiometry with ion-selective electrodes). While electrophysiology and electrochemistry differ in the brain systems that they probe, they are similar in practice. With the exception of surface electrophysiological techniques (e.g., electroencephalography), both electrophysiology and electrochemistry in vivo involve the implantation of electrodes, allowing for highly spatially resolved measurements of brain communication events.

The invasive act of electrode implantation triggers an immune response in the brain that alters electrode performance over time, an effect generally referred to as biofouling. Biofouling causes two major changes in the properties of the implanted electrodes: (1) increased impedance, which affects all implanted electrodes, and (2) polarization, specifically of the reference electrode. The increase in impedance can have adverse effects on the recording quality of implanted electrodes, both in electrophysiology and electrochemistry. As a result, numerous successful efforts have been made toward both reducing the native impedance of implantable electrodes and mitigating the increase in impedance that occurs after implantation [2–5]. The other major consequence of biofouling is reference electrode polarization, defined herein as a change in the reference electrode potential from its original value. This reference electrode polarization is particularly detrimental to in vivo electrochemistry, as the selectivity and sensitivity of the technique depend on the accuracy of the applied potentials. To date, no efforts to mitigate biofouling-induced reference electrode polarization have yielded success for longer than 4 weeks [6–8]. Mitigating reference electrode polarization over longer periods of time (e.g., months to years) would allow for more accurate measurements in studies that benefit from long-term experimentation, such as those on progressive neurological disorders (e.g., Parkinson’s disease).

In this review, we describe the causes and effects of chronic electrode biofouling, particularly with respect to reference electrodes and in vivo electrochemistry. Special attention is given to biocompatible reference electrodes, as the cytotoxicity of the widely used Ag/AgCl reference electrode [9–12] exacerbates the immune response to implantation, intensifies the resultant biofouling and polarization, and prohibits the use of Ag/AgCl in humans. Promising biocompatible reference electrode materials (e.g., iridium oxide, boron-doped diamond) are introduced and discussed in detail. The field of in vivo electrochemistry is moving toward a greater emphasis on chronic experiments. To maximize the success, validity, and safety of these experiments, a move toward more widespread use of biocompatible reference electrodes is critical. These electrodes should reduce the extent to which the brain is perturbed by implantation and enable high-fidelity measurements over longer periods of time. The goals of this review are to bring attention to the longstanding challenge of biofouling in chronic in vivo electrochemistry, suggest and

describe biocompatible reference electrode materials that can mitigate chronic biofouling, and encourage further characterization of these electrodes.

Immune response to electrode implantation in the brain

The introduction of an electrode into the brain causes acute injury. The tissue suffers mechanical strain and tearing, the blood–brain barrier (BBB) is ruptured, and the movement of signaling molecules is impeded, both sterically and via diminished perfusion [13, 14]. Nearby glial cells (e.g., microglia, astrocytes) are immediately activated by the BBB rupture-induced influx of blood–serum proteins (e.g., albumin) [13, 14]. Kozai et al. used two-photon microscopy in mice to better understand the timeline of the immune response to electrode implantation and found that, within 1 h of implanting a four-shank Michigan probe, activated microglia extended processes at an approximate rate of 1.6 μm/min toward the injury site and began encapsulation of the probe with lamellipodia [15]. After 12 to 24 h, activated microglia become motile and the cell bodies migrate toward the probe for further encapsulation [13, 15, 16]. This is followed by encapsulation by reactive (i.e., activated) astrocytes and, by 2 to 4 weeks post-implantation, the probe is encapsulated by a glial sheath that becomes more compact and tightly networked over time [16–18]. The general timeline of the immune response to electrode implantation in the brain is illustrated in Fig. 1 [19].

Impedance and its impact on in vivo electrophysiology

The encapsulating glial sheath from the immune response to electrode implantation (vide supra) acts as a diffusion barrier [20] that limits ionic exchange and electron transfer between the electrode and surrounding media, altering electrode performance over time (i.e., biofouling). One major consequence of biofouling is increased electrode impedance [5, 21–25], which can adversely affect both electrophysiological and electrochemical measurements in vivo, though the extent to which it affects the performance of electrophysiological electrodes (e.g., signal-to-noise ratio) is debated. Several studies show that electrophysiological electrode performance is inversely related to electrode impedance (i.e., low-impedance electrodes exhibit better performance) [2–4, 26–31]. This is often attributed to the fact that thermal noise, one of the main noise sources in microelectrode recordings, is proportional to the square root of the real component of electrode impedance (Eq. 1).

$$V_{\mathrm{rms}}^{\mathrm{th}} = \sqrt{4k_{\mathrm{B}}TZ_{\mathrm{real}}\Delta f} \tag{1}$$

In Eq. 1, $V_{\mathrm{rms}}^{\mathrm{th}}$ is the root mean square thermal noise, k_{B} is Boltzmann's constant, T is temperature, Z_{real} is the average of the real component of impedance, and Δf is the bandwidth over which the measurements are made. Counterarguments assert that electrode impedance is not a major determinant of performance as long as the impedance falls within the range of standard polytrodes (~ 100 kΩ to 2 MΩ) [32]. This dichotomy may be explained by variations in the electrode types and amplifiers used across studies that investigate this relationship. The type of electrode is a key factor that influences the extent to which impedance determines electrode performance. Shunt capacitance, a combination

of all capacitances from electrode tip to amplifier input, is strongly related to electrode type. For electrode designs with relatively long, thinly insulated electrode wires (e.g., single microwires, tetrodes), shunt capacitance is a significant source of signal degradation that can be mitigated by reducing electrode impedance [33]. In contrast, shunt capacitance is much lower for silicon polytrodes [34], rendering electrode impedance less influential on performance in such cases.

Another important factor is the input impedance of the amplifier. An electrode connected to an amplifier effectively forms a voltage divider and the signal loss due to this effect can be calculated with Eq. 2.

$$V_{\text{out}} = \frac{V_{\text{in}} Z_2}{(Z_1 + Z_2)} \tag{2}$$

In Eq. 2, V_{in} is the voltage sensed by the electrode, Z_1 and Z_2 are the impedances of the electrode and amplifier, respectively, and V_{out} is the measured voltage. Ideally, the amplifier input impedance is much higher than that of the electrode to minimize signal loss due to this voltage divider effect. For example, Intan Technologies RHD2000-series amplifier microchips have an input impedance of 13 MΩ at 1 kHz [35]. Using such an amplifier to record neural activity from an electrode with an impedance of 100 kΩ would result in a relatively negligible signal loss of 0.8% from the voltage divider effect. However, using the same amplifier to record from an electrode with an impedance of 2 MΩ would result in a much more evident signal loss of 13%. An amplifier with a lower input impedance would exacerbate this effect. Thus, variation in the electrode types and amplifiers used across different studies likely complicates direct comparisons of the extent to which electrode impedance influences electrophysiological recording performance. Nevertheless, since in vivo electrode impedance changes are an indicator of the immune response to implantation, reduction of in vivo electrode impedance is typically an indicator of improved biocompatibility. This is a positive outcome, even in cases where performance enhancements are minor.

Efforts toward improving electrophysiological electrode performance are typically focused on the working (i.e., sensing) electrode, with less attention given to the reference electrode. This is also generally the case for in vivo electrochemistry, despite the fact that chronic reference electrode potential stability is imperative. Electrochemical measurements rely on accurately applied potentials, which depend on a stable reference electrode potential. Chronic polarization of the reference electrode is a major result of biofouling that diminishes the selectivity and sensitivity of in vivo electrochemistry [5, 7]. We now shift focus from electrophysiology to electrochemistry and highlight the importance of long-term stabilization of the reference electrode potential in vivo.

Effects of biofouling on chronic in vivo electrochemistry

Fast-scan cyclic voltammetry (FSCV) is one of the most widely used electrochemical methods for neurotransmitter detection in vivo. There are numerous review articles that explain the principles behind FSCV [36–39]. To date, the majority of in vivo FSCV studies

have been acute (i.e., minutes to hours), but there have been chronic (i.e., days or longer) studies that have pushed the temporal boundaries of in vivo neurochemical measurements. The timescales of acute and chronic studies described throughout this review refer to the time over which the electrodes are implanted and used to make measurements. By this definition, a month-long study involving the implantation of new electrodes for each measurement would not be considered a chronic study. Chronic dopamine detection via FSCV was performed by Clark et al. in rats and mice over the course of months [40], by Schwerdt et al. in non-human primates for months [41], and by Schwerdt et al. in rats for over a year [42]. Recordings on this timescale are vital to better understanding progressive neurological disorders, as they typically develop gradually over months or years.

A large background signal is generated from FSCV due to non-Faradaic contributions from the high scan rate and Faradaic contributions from the redox of electroactive species on and around the electrode [43]. When a change in the concentration of the analyte of interest (e.g., dopamine) occurs, the background signal is subtracted, resulting in a cyclic voltammogram specific to that analyte. Accuracy in the potentials of the signal is paramount, as the background-subtracted cyclic voltammogram serves as a chemical identifier of the analyte. Thus, the potentials of the FSCV background signal must be accurate and stable over the course of the study for reliable analyte identification and quantification.

The potentials of the FSCV background signal do not shift appreciably on the timescale of acute studies, but biofouling over the course of chronic studies results in substantial background signal potential shifts that worsen over time and diminish analyte selectivity and sensitivity [5, 7]. This chronic potential shift is often compensated for by applying a potential offset to the FSCV waveform [40–42]. The value of the applied potential offset (typically + 100 to 300 mV) varies across laboratories, researchers, animals, and implantation time, as it is chosen qualitatively. In practice, when a shift in the FSCV background signal is apparent, the potential offset is applied and the shape of the FSCV background signal is evaluated. If necessary, the value of the offset is changed until a desired shape is achieved. While this potential offset strategy is commonly utilized in chronic in vivo FSCV studies, it is not an ideal solution because it lacks quantitative rigor and the timescale and magnitude of the potential shift is variable [5]. Seaton et al. showed that there are two major biofouling-induced factors that contribute to chronic FSCV potential shifts in vivo: (1) increased electrode impedance of both the working and reference electrodes and (2) polarization of the reference electrode [5]. They showed that the utilization of a counter electrode and three-electrode potentiostat improves chronic FSCV signal fidelity in vivo by mitigating the increase in impedance, but reference electrode polarization remains an issue. Polarization of the reference electrode is typically not measured directly in chronic in vivo FSCV studies, and the potential offset strategy (vide supra) is used qualitatively to compensate for the combined effect of increased impedance and reference electrode polarization. A more comprehensive solution to the chronic FSCV background signal shift is thus necessary, ideally involving a counter electrode for impedance mitigation and a biocompatible reference electrode for polarization mitigation.

As with most other current in vivo electrochemical techniques, FSCV most commonly utilizes the Ag/AgClpseudo-reference electrode [36, 44, 45]. Unlike a commercial Ag/AgCl

reference electrode, which is unsuitable for in vivo use due to its size and required maintenance, the Ag/AgClpseudo-reference electrode is composed of a AgCl-coated Ag wire with no internal solution compartment. Such an electrode can be fabricated by soaking Ag wire in sodium hypochlorite (i.e., bleach), though electroplating and other methods of chloridizing the Ag wire are also common. The Ag/AgClpseudo-reference electrode is referred to as Ag/AgCl throughout this review for ease of reading, and it is characterized by the following reaction:

$$\mathrm{AgCl}(s) + e^- \rightleftharpoons \mathrm{Ag}(s) + \mathrm{Cl}^- \tag{3}$$

Equation 4 describes the dependence of the Ag/AgCl electrode potential on chloride ion activity.

$$E = E^0 - \frac{RT}{F}\ln(a_{\mathrm{Cl}^-}) \tag{4}$$

In Eq. 4, E is the potential of the Ag/AgCl electrode, E^0 is the standard potential of the Ag/AgCl electrode, R is the ideal gas constant, T is temperature, F is Faraday's constant, and a_{Cl^-} is chloride ion activity. Since the chloride concentration in vivo does not fluctuate appreciably, there exists a stable chloride equilibrium between a freshly implanted Ag/AgCl electrode and the surrounding media. This is the basis for the stability of the Ag/AgCl reference electrode potential over the course of acute studies. However, the biofouling that occurs during chronic studies results in decreased surface chlorine on the Ag/AgCl electrode [5–7]. This can be seen in Fig. 2, which shows the encapsulation of a Ag/AgCl reference electrode after 3 weeks of brain implantation [5].

The chloride equilibrium required for Ag/AgCl potential stability is disrupted by the encapsulating sheath, resulting in chronic polarization of the electrode [5, 6, 8]. While there have been successful efforts toward mitigating chronic Ag/AgCl reference electrode polarization in vivo, none have been successful for longer than 4 weeks [6–8]. In addition, Ag and AgCl are highly cytotoxic in the brain and other tissue [9–12], exacerbating the immune response to implantation and prohibiting the use of Ag/AgCl in humans. Due to its favorable electrochemical properties and simplicity of fabrication, Ag/AgCl is currently the most commonly used reference electrode for FSCV. However, the issues of cytotoxicity and chronic potential instability in vivo warrant the investigation of other reference electrode materials. Replacing the Ag/AgCl reference electrode with a stable, biocompatible reference electrode should mitigate reference electrode polarization and provide a chronically stable, high-fidelity FSCV signal when utilized in a three-electrode configuration for impedance mitigation (vide supra). The importance of such a reference electrode is not limited to FSCV, as any in vivo electrochemical technique involving prolonged electrode implantation will benefit from enhanced reference electrode potential stability and biocompatibility.

Toward reference electrodes with superior biocompatibility and potential stability

One of the most important aspects shaping the future of in vivo electrochemistry is the improvement of chronic measurements. In addition, there is an increasing interest in performing these measurements in humans. Thus, a shift toward the use of biocompatible reference electrodes that are non-toxic and provide potential stability over the course of long-term experimentation is imperative. There are several implantable, biocompatible reference electrodes that have shown promise in vitro and in vivo. The most prominent candidates, iridium oxide and boron-doped diamond, are discussed in detail below.

Iridium oxide

Iridium oxide (IrOx) is a biocompatible material used to construct neural stimulation and recording electrodes, pH sensors, and reference electrodes. Below, we describe the electrochemical properties, biocompatibility, fabrication methods, and applications of IrOx. The IrOx electrode is primarily characterized by the following reaction:

$$2IrO_2 + 2H^+ + 2e^- \rightleftharpoons Ir_2O_3 + H_2O \quad (5)$$

Equation 6 describes the dependence of the IrOx electrode potential on proton activity.

$$E = E^0 - \frac{RT}{F}\ln(a_{H^+}) \quad (6)$$

In Eq. 6, E is the potential of the IrOx electrode, E^0 is the standard potential of the IrOx electrode, R is the ideal gas constant, T is temperature, F is Faraday's constant, and a_{H^+} is proton activity. IrOx electrodes have a theoretically Nernstian dependence on pH. In practice, the pH response ranges from Nernstian (− 59 mV/pH unit) to super-Nernstian (ca. − 80 mV/pH unit), depending on the fabrication method and resultant oxidation state and thickness of the IrOx film [46]. Due to this pH sensitivity, IrOx electrodes are commonly used as pH probes, both in vitro and in vivo [47–56]. In addition, the high charge injection capacity of IrOx electrodes has led to their frequent use in neural stimulation and recording [57–66]. While scarce in comparison, there are reports on the use of IrOx as reference electrodes [67–72]. The strict regulation of pH in vivo, particularly in the brain (7.2 to 7.4) [73], provides the environment for a stable IrOx reference electrode potential.

The biocompatibility of IrOx is well-documented and is one of the most important advantages IrOx holds over Ag/AgCl for use in vivo [74–79]. Unlike Ag/AgCl, IrOx releases no toxic elements into the body. Additionally, IrOx is known to catalyze the decomposition of hydrogen peroxide, which is commonly produced at metal surfaces during corrosion and has an inflammatory effect on biological tissue [74, 80]. The ability of IrOx to promote the conversion of hydrogen peroxide into water and oxygen has been proposed as a key factor in its biocompatibility [74]. In contrast to the toxicity of Ag/AgCl, which causes biofouling-induced disruption of the chloride equilibrium between electrode and media

(vide supra), the biocompatibility of IrOx should minimize proton equilibrium disruption, resulting in a chronically stable reference electrode potential in vivo. There are four common methods of IrOx electrode fabrication: thermal, sputtered, activated, and electrodeposited IrOx film. The method and relevant parameters of IrOx electrode fabrication determine the surface morphology of the IrOx film (Fig. 3) [81–84], which in turn determines the electrochemical properties of the electrode. These IrOx fabrication methods are described below.

The process for producing thermal IrOx film (TIROF) generally involves dipping an electrode into an iridium salt solution, drying at room temperature or slightly higher, then annealing at high temperature (> 300 °C) [85]. This process can be repeated several times to produce a multilayered IrOx film. The annealing step for the final layer is typically done for several hours. Fig. 3A shows TIROF on a Ti electrode prepared to investigate the effects of various coatings on the performance of stimulating electrodes [81]. It was found that the exceptional charge storage capacity of IrOx stimulating electrodes could be further improved by the integration of nickel into the film. TIROF offers a tradeoff between simplicity and tunability: it is the simplest IrOx fabrication method and does not require expensive instrumentation (e.g., sputtering system, potentiostat), but it does not provide the same level of film customization as other methods.

In contrast to the relative simplicity of TIROF is sputtered IrOx film (SIROF), produced by reactive sputtering of Ir onto an electrode in oxygen-rich plasma [86]. The equipment required for SIROF is expensive and sophisticated, but it provides the capability to fine-tune the film. Fig. 3B shows SIROF deposited onto Ti–Pt in a study investigating the effects of changing carrier gas flow and pumping speeds on the morphological and electrochemical properties of SIROF [82]. These tunable sputtering parameters allow for control over the extent of oxygen integration in the film, which has a substantial influence on the morphology and electrochemical characteristics of the SIROF [82, 87].

Activated IrOx film (AIROF) is produced by electrochemical oxidation of an Ir electrode [88]. The process involves the application of a potential waveform to an Ir electrode in a solution such as phosphate-buffered saline (PBS), Na_2HPO_4, or H_2SO_4. Fig. 3C shows AIROF, produced by sweeping the potential of an Ir electrode from − 1.0 to 1.0 V vs. Ag/AgCl at 0.05 Hz in 0.9% NaCl, in an analysis on how the number of activation cycles affects the electrochemical properties of AIROF [83]. The study found that AIROF charge storage capacity increases, and impedance decreases, as the number of activation cycles is increased. Other factors that influence AIROF morphology and the resultant electrochemical properties are the activation solution components and the shape, potential limits, and frequency of the applied waveform.

Like AIROF, electrodeposited IrOx film (EIROF) is produced electrochemically. Whereas AIROF involves the oxidation of an Ir electrode, EIROF is produced by electrodeposition of IrOx from an Ir-containing solution onto a non-Ir electrode [89]. The electrodeposition parameters and solution components vary across studies and allow for customization of the EIROF. Fig. 3D shows EIROF produced by applying a constant potential (0.6 V vs. Ag/AgCl) to a Pt electrode in an $IrCl_4$ solution to investigate how the combination of

nano-structures and coatings can improve the performance of stimulating electrodes [84]. It was found that applying a nanocone-shaped Pt gray coating to the Pt electrode, prior to IrOx electrodeposition, increased the surface area of the electrode and allowed for better IrOx adhesion during electrodeposition. This resulted in superior mechanical and electrochemical properties (e.g., higher charge storage capacity, lower impedance) of the IrOx/Pt gray composite electrode, compared to bare Pt, Pt gray, or IrOx alone.

Two of the most common implantable electrode designs, the Utah array and Michigan probe, include IrOx electrodes fabricated with SIROF and AIROF, respectively. Given the morphological differences between SIROF and AIROF (Fig. 3B, C), differences in their electrochemical properties should be expected. These differences were investigated by Franklin et al., who compared the impedance and potential stability of SIROF and AIROF electrodes [71]. AIROF electrodes were activated by applying a 1-Hz square wave between − 0.85 and + 0.9 V vs. SCE for 200 cycles in either PBS or Na_2HPO_4. The 1-kHz impedance and open circuit potential of the electrodes were measured periodically as they soaked in PBS. While the SIROF electrodes exhibited the least variation in impedance over time, the AIROF electrodes (both PBS- and Na_2HPO_4-activated) were superior in terms of potential stability, making them more attractive for use as reference electrodes.

The Na_2HPO_4-activated AIROF electrodes had the highest potential stability during the PBS soak test (3.2 mV drift per day, over 8 days) and were thus employed as reference electrodes, with Pt working and counter electrodes, for in vitro dopamine measurement via cyclic voltammetry (Fig. 4) [71]. Figure 4A contains cyclic voltammograms for 10 mM dopamine in PBS at scan rates ranging from 50 mV/s to 10 V/s. The same setup was used at a scan rate of 1 V/s to measure dopamine ranging from 0.1 to 10 mM (Fig. 4B). A linear calibration curve was generated, and the dopamine sensitivity was calculated to be 5.85 nA/mM. While this sensitivity is insufficient for in vivo dopamine detection, a higher scan rate (e.g., 400 V/s for FSCV) would considerably enhance sensitivity. It is unknown whether scan rates higher than 10 V/s were attempted.

In addition to chronic potential stability, the noise produced by the reference electrode is critical, as it has a direct effect on the sensitivity of the electrochemical probe. Tolosa et al. demonstrated that on-probe IrOx reference electrodes produce less noise than separate Ag/AgCl reference electrodes when used with glutamate biosensors [72]. Utilization of the on-probe IrOx reference electrode reduced the baseline noise at the glutamate oxidase-modified Pt working electrode by 61% in vitro and 71% in vivo when compared to the utilization of a separate Ag/AgCl reference electrode. Since an on-probe reference electrode design inherently lowers noise, a noise comparison between IrOx and Ag/AgCl reference electrodes that are both on-probe, or both separate, would be even more elucidating. Overall, the biocompatibility, potential stability, and low noise of the IrOx electrode make it highly attractive for use in vivo, but the effects of chronic implantation on its performance as a reference electrode have yet to be studied in depth.

Metals, alloys, and semimetals (e.g., boron-doped diamond)

Metals and alloys (e.g., Pt, Pt–Ir, stainless steel) can be used unmodified as pseudo-reference electrodes, but unlike Ag/AgCl or IrOx, they do not have well-defined redox couples.

Chronic brain implantation presents further complications, as the direction and extent of polarization due to biofouling has not been studied for these materials. Stainless steel has the additional drawback of elemental composition variability, which further confounds its potential, though there are several reports on its use as a reference electrode in vivo for electrochemical measurements [90–97]. Boron-doped diamond (BDD), often referred to as a "semimetal", is a highly biocompatible and customizable material with several advantageous electrochemical properties, including a wide potential window, low background current, and tunability via controllable surface termination (i.e., hydrogen- vs. oxygen-terminated BDD) [98]. The use of BDD in vivo is on the rise, but it is typically limited to the working electrode [95, 99–105]. Of the few reports on the use of BDD reference electrodes [106–110], only one [110] has involved in vivo implantation.

Although the redox couple that defines the potential of a BDD reference electrode is undefined, there does appear to be a pH dependence. The BDD reference potential becomes more cathodic (i.e., negative) with increasing pH, but the response is non-Nernstian [106, 109]. Thus, the BDD potential is defined in part by a proton equilibrium between the electrode and surrounding media. This may imply a difference in potential stability between hydrogen- and oxygen-terminated BDD, though we are not aware of any studies that have made this comparison. As with IrOx, such a pH dependence is advantageous for BDD reference electrodes in the brain, where pH is strictly regulated (vide supra).

Intrinsic (i.e., non-doped) diamond is a well-known biocompatible material [111–118]. In the case of BDD, the stability of boron dopant atoms within the diamond lattice results in a negligible amount of free boron [119], which is not a highly toxic element [120]. As a result, BDD is highly biocompatible [121–127]. In fact, a positive correlation between boron content and biocompatibility of diamond films (e.g., cell adhesion and viability) has been shown and is attributed to differences in surface potential that can influence the adsorption and conformation of proteins on the BDD surface [121, 122].

BDD electrode fabrication involves the use of chemical vapor deposition (CVD) or microwave plasma-assisted chemical vapor deposition (MPCVD) to deposit BDD film onto a substrate. Typical growth conditions involve plasma temperatures around 2500 K, substrate temperatures around 1200 K, and pressures around 25 mbar [128]. Suitable substrate materials are limited to those that can handle such extreme conditions (e.g., Si, Nb, Mb, Ti, Ta, W) [129]. BDD electrode geometry is highly customizable and dependent on the growth conditions. BDD is commonly left on the growth substrate as a thin film, but thicker BDD (> 100 μm) can be removed from the growth substrate, resulting in freestanding BDD that can be laser micromachined into various three-dimensional geometries [128, 129].

In addition to the geometry and surface termination, the side of the BDD (i.e., nucleation side vs. growth side) used for sensing has a profound effect on the electrochemical properties of the electrode. "Nucleation side" refers to the interface between the BDD film and substrate, whereas "growth side" refers to the outermost surface of the film. Methods for transferring BDD onto flexible substrates (e.g., polyimide, polynorbornene, parylene) typically allow for exposure of the BDD nucleation side only [108, 130, 131]. However, Fan et al. recently developed a method for BDD transfer onto Parylene C that allows for

exposure of the BDD growth side, which exhibits a rougher surface morphology, a higher sp^3/sp^2 carbon ratio, and better boron doping than the nucleation side (Fig. 5) [110].

As a result of these superior surface characteristics, the growth side displayed comparatively lower impedance and background current, faster electron transfer kinetics, and higher dopamine fouling resistance. It would be reasonable to presume that the growth side would also exhibit better open circuit potential stability than the nucleation side, though this comparison was not made. Using square wave voltammetry in vitro with the flexible sensor consisting of BDD-growth-side working, reference, and counter electrodes, dopamine was successfully detected in the presence of ascorbic acid, a well-known biological interferent. The probe was also used in vivo to detect visual stimulus-induced neural activity. BDD is a promising in vivo reference electrode candidate because of its biocompatibility, favorable electrochemical properties, and wide range of possible electrode geometries. Future work should focus on better understanding the reactions that define the potential of BDD and any changes that occur over the course of chronic in vivo implantation.

Conclusions

Biofouling is a prevalent issue in studies that involve chronic implantation of electrodes. In electrochemical measurements, the increase in electrode impedance that occurs due to biofouling has been successfully mitigated previously, but the challenge of reference electrode polarization is still largely unsolved. Due to the chronic potential instability and toxicity of the commonly used Ag/AgCl reference electrode in vivo, a move toward more stable, biocompatible reference electrode materials is warranted. Two promising candidates, iridium oxide (IrOx) and boron-doped diamond (BDD), were highlighted and discussed in detail. Since neither material has been studied extensively for use as reference electrodes in vivo, there is much room for investigation and direct comparison. The tunability of both IrOx and BDD bodes well for determining optimal fabrication protocols for maximum potential stability. Utilizing a biocompatible reference electrode (to mitigate chronic polarization) in a three-electrode configuration (to mitigate increased impedance) should offer a stable electrochemical system for chronic in vivo measurements. As in vivo measurements continue to advance toward more chronic experimentation, both in animal models and humans, understanding and utilizing biocompatible reference electrodes will become increasingly crucial.

Acknowledgements

The authors thank Dr. Stephen L. Cowen (Department of Psychology, University of Arizona) for his insight and advice, particularly on the topic of electrophysiology.

Funding

This work was funded by NIH, award number R01 NS112176.

References

1. Swammerdam J The book of nature. London: C. G. Seyffert; 1758.
2. Ferguson JE, Boldt C, Redish AD. Creating low-impedance tetrodes by electroplating with additives. Sensors Actuators, A Phys. 2009; 10.1016/j.sna.2009.10.001.

3. Desai SA. Improving impedance of implantable microwire multi-electrode arrays by ultrasonic electroplating of durable platinum black. Front Neuroeng. 2010. 10.3389/fneng.2010.00005.
4. Chung T, Wang JQ, Wang J, Cao B, Li Y, Pang SW. Electrode modifications to lower electrode impedance and improve neural signal recording sensitivity. J Neural Eng. 2015. 10.1088/1741-2560/12/5/056018.
5. Seaton BT, Hill DF, Cowen SL, Heien ML. Mitigating the effects of electrode biofouling-induced impedance for improved long-term electrochemical measurements in vivo. Anal Chem. 2020. 10.1021/acs.analchem.9b05194.
6. Moussy F, Harrison DJ. Prevention of the rapid degradation of subcutaneously implanted Ag/AgCl reference electrodes using polymer coatings. Anal Chem. 1994. 10.1021/ac00077a015.
7. Hashemi P, Walsh PL, Guillot TS, Gras-Najjar J, Takmakov P, Crews FT, Wightman RM. Chronically implanted, Nafion-coatedAg/AgCl reference electrodes for neurochemical applications. ACS Chem Neurosci. 2011. 10.1021/cn2000684.
8. Wang B, Yang P, Ding Y, Qi H, Gao Q, Zhang C. Improvement of the biocompatibility and potential stability of chronically implanted electrodes incorporating coating cell membranes. ACS Appl Mater Interfaces. 2019. 10.1021/acsami.8b20542.
9. Dymond AM, Kaechele LE, Jurist JM, Crandall PH. Brain tissue reaction to some chronically implanted metals. J Neurosurg. 1970. 10.3171/jns.1970.33.5.0574.
10. Stensaas SS, Stensaas LJ. Histopathological evaluation of materials implanted in the cerebral cortex. Acta Neuropathol. 1978. 10.1007/BF00689766.
11. Jackson WF, Duling BR. Toxic effects of silver-silver chloride electrodes on vascular smooth muscle. Circ Res 1983. 10.1161/01.RES.53.1.105.
12. Yuen TGH, Agnew WF, Bullara LA. Tissue response to potential neuroprosthetic materials implanted subdurally. Biomaterials. 1987. 10.1016/0142-9612(87)90103-7.
13. Kozai TDY, Jaquins-Gerstl AS, Vazquez AL, Michael AC, Cui XT. Brain tissue responses to neural implants impact signal sensitivity and intervention strategies. ACS Chem Neurosci. 2015. 10.1021/cn500256e.
14. Kozai TDY, Marzullo TC, Hooi F, Langhals NB, Majewska AK, Brown EB, Kipke DR. Reduction of neurovascular damage resulting from microelectrode insertion into the cerebral cortex using in vivo two-photon mapping. J Neural Eng. 2010. 10.1088/1741-2560/7/4/046011.
15. Kozai TDY, Vazquez AL, Weaver CL, Kim SG, Cui XT. In vivo two-photon microscopy reveals immediate microglial reaction to implantation of microelectrode through extension of processes. J Neural Eng. 2012. 10.1088/1741-2560/9/6/066001.
16. Szarowski DH, Andersen MD, Retterer S, Spence AJ, Isaacson M, Craighead HG, Turner JN, Shain W. Brain responses to micromachined silicon devices. Brain Res. 2003. 10.1016/S0006-8993(03)03023-3.
17. Biran R, Martin DC, Tresco PA. Neuronal cell loss accompanies the brain tissue response to chronically implanted silicon microelectrode arrays. Exp Neurol. 2005. 10.1016/j.expneurol.2005.04.020.
18. Kozai TDY, Gugel Z, Li X, Gilgunn PJ, Khilwani R, Ozdoganlar OB, Fedder GK, Weber DJ, Cui XT. Chronic tissue response to carboxymethyl cellulose based dissolvable insertion needle for ultra-small neural probes. Biomaterials. 2014. 10.1016/j.biomaterials.2014.07.039.
19. Campbell A, Wu C. Chronically implanted intracranial electrodes: tissue reaction and electrical changes. Micromachines. 2018. 10.3390/mi9090430.
20. Roitbak T, Syková E. Diffusion barriers evoked in the rat cortex by reactive astrogliosis. Glia. 1999. 10.1002/(SICI)1098-1136(199910)28:1<40::AID-GLIA5>3.0.CO;2-6.
21. Grill WM, Thomas MJ. Electrical properties of implant encapsulation tissue. Ann Biomed Eng. 1994. 10.1007/BF02368219.
22. Williams JC, Hippensteel JA, Dilgen J, Shain W, Kipke DR. Complex impedance spectroscopy for monitoring tissue responses to inserted neural implants. J Neural Eng. 2007. 10.1088/1741-2560/4/4/007.
23. Mercanzini A, Colin P, Bensadoun J-C, Bertsch A, Renaud P. In vivo electrical impedance spectroscopy of tissue reaction to microelectrode arrays. IEEE Trans Biomed Eng. 2009. 10.1109/TBME.2009.2018457.

24. Lempka SF, Miocinovic S, Johnson MD, Vitek JL, McIntyre CC. In vivo impedance spectroscopy of deep brain stimulation electrodes. J Neural Eng. 2009. 10.1088/1741-2560/6/4/046001.
25. Meunier CJ, Denison JD, McCarty GS, Sombers LA. Interpreting dynamic interfacial changes at carbon fiber microelectrodes using electrochemical impedance spectroscopy. Langmuir. 2020. 10.1021/acs.langmuir.9b03941.
26. Keefer EW, Botterman BR, Romero MI, Rossi AF, Gross GW. Carbon nanotube coating improves neuronal recordings. Nat Nanotechnol. 2008. 10.1038/nnano.2008.174.
27. Ludwig KA, Langhals NB, Joseph MD, Richardson-Burns SM, Hendricks JL, Kipke DR. Poly(3,4-ethylenedioxythiophene) (PEDOT) polymer coatings facilitate smaller neural recording electrodes. J Neural Eng. 2011. 10.1088/1741-2560/8/1/014001.
28. Ansaldo A, Castagnola E, Maggiolini E, Fadiga L, Ricci D. Superior electrochemical performance of carbon nanotubes directly grown on sharp microelectrodes. ACS Nano. 2011. 10.1021/nn103445d.
29. Du J, Blanche TJ, Harrison RR, Lester HA, Masmanidis SC. Multiplexed, high density electrophysiology with nanofabricated neural probes. PLoS One. 2011. 10.1371/journal.pone.0026204.
30. Scott KM, Du J, Lester HA, Masmanidis SC. Variability of acute extracellular action potential measurements with multisite silicon probes. J Neurosci Methods. 2012. 10.1016/j.jneumeth.2012.08.005.
31. Zhao Z, Gong R, Zheng L, Wang J. In vivo neural recording and electrochemical performance of microelectrode arrays modified by rough-surfaced AuPt alloy nanoparticles with nanoporosity. Sensors (Switzerland). 2016. 10.3390/s16111851.
32. Neto JP, Baião P, Lopes G, Frazão J, Nogueira J, Fortunato E, Barquinha P, Kampff AR. Does impedance matter when recording spikes with polytrodes? Front Neurosci. 2018. 10.3389/fnins.2018.00715.
33. Robinson DA. The electrical properties of metal microelectrodes. Proc IEEE. 1968. 10.1109/PROC.1968.6458.
34. Obien MEJ, Deligkaris K, Bullmann T, Bakkum DJ, Frey U. Revealing neuronal function through microelectrode array recordings. Front Neurosci. 2015. 10.3389/fnins.2014.00423.
35. RHD2000 Datasheet. http://intantech.com/files/Intan_RHD2000_series_datasheet.pdf. Accessed 31 Jan 2021.
36. Rodeberg NT, Sandberg SG, Johnson JA, Phillips PEM, Wightman RM. Hitchhiker's guide to voltammetry: acute and chronic electrodes for in vivo fast-scan cyclic voltammetry. ACS Chem Neurosci. 2017. 10.1021/acschemneuro.6b00393.
37. Roberts JG, Sombers LA. Fast-scan cyclic voltammetry: chemical sensing in the brain and beyond. Anal Chem. 2018. 10.1021/acs.analchem.7b04732.
38. Venton BJ, Cao Q. Fundamentals of fast-scan cyclic voltammetry for dopamine detection. Analyst. 2020. 10.1039/c9an01586h.
39. Puthongkham P, Venton BJ. Recent advances in fast-scan cyclic voltammetry. Analyst. 2020. 10.1039/c9an01925a.
40. Clark JJ, Sandberg SG, Wanat MJ, Gan JO, Horne EA, Hart AS, Akers CA, Parker JG, Willuhn I, Martinez V, Evans SB, Stella N, Phillips PEM. Chronic microsensors for longitudinal, subsecond dopamine detection in behaving animals. Nat Methods. 2010. 10.1038/nmeth.1412.
41. Schwerdt HN, Shimazu H, Amemori K, Amemori S, Tierney PL, Gibson DJ, Hong S, Yoshida T, Langer R, Cima MJ, Graybiel AM. Long-term dopamine neurochemical monitoring in primates. Proc Natl Acad Sci U S A. 2017. 10.1073/pnas.1713756114.
42. Schwerdt HN, Zhang E, Kim MJ, Yoshida T, Stanwicks L, Amemori S, Dagdeviren HE, Langer R, Cima MJ, Graybiel AM. Cellular-scale probes enable stable chronic subsecond monitoring of dopamine neurochemicals in a rodent model. Commun Biol. 2018. 10.1038/s42003-018-0147-y.
43. Meunier CJ, Roberts JG, McCarty GS, Sombers LA. Background signal as an in situ predictor of dopamine oxidation potential: improving interpretation of fast-scan cyclic voltammetry data. ACS Chem Neurosci. 2017. 10.1021/acschemneuro.6b00325.

44. Phillips PEM, Robinson DL, Stuber GD, Carelli RM, Wightman RM. Real-time measurements of phasic changes in extracellular dopamine concentration in freely moving rats by fast-scan cyclic voltammetry. Methods Mol Med. 2003. 10.1385/1-59259-358-5:443.
45. Roberts JG, Lugo-Morales LZ, Loziuk PL, Sombers LA. Real-time chemical measurements of dopamine release in the brain. Methods Mol Biol. 2013. 10.1007/978-1-62703-251-3_16.
46. Głąb S, Hulanicki A, Edwall G, Folke F, Ingman I, Koch WF. Metal-metal oxide and metal oxide electrodes as pH sensors. Crit Rev Anal Chem. 1989. 10.1080/10408348908048815.
47. Kinoshita K, Madou MJ. Electrochemical measurements on Pt, Ir, and Ti oxides as pH probes. J Electrochem Soc. 1984. 10.1149/1.2115755.
48. Papeschi G, Merigliano S, Zaninotto G, Baessato M, Ancona E, Larini M. The iridium/iridium oxide electrode to in vivo measurement of oesophageal and gastric pH. J Med Eng Technol. 1984. 10.3109/03091908409032080.
49. Kinlen PJ, Heider JE, Hubbard DE. A solid-state pH sensor based on a Nafion-coated iridium oxide indicator electrode and a polymer-based silver chloride reference electrode. Sensors Actuators B Chem. 1994. 10.1016/0925-4005(94)01254-7.
50. Marzouk SAM, Ufer S, Buck RP, Johnson TA, Dunlap LA, Cascio WE. Electrodeposited iridium oxide pH electrode for measurement of extracellular myocardial acidosis during acute ischemia. Anal Chem. 1998. 10.1021/ac980608e.
51. Suzuki H, Arakawa H, Sasaki S, Karube I. Micromachined Severinghaus-type carbon dioxide electrode. Anal Chem. 1999. 10.1021/ac9811468.
52. Wipf DO, Ge F, Spaine TW, Baur JE. Microscopic measurement of pH with iridium oxide microelectrodes. Anal Chem. 2000. 10.1021/ac000383j.
53. Marzouk SAM, Buck RP, Dunlap LA, Johnson TA, Cascio WE. Measurement of extracellular pH, K+, and lactate in ischemic heart. Anal Biochem. 2002. 10.1016/S0003-2697(02)00220-8.
54. Bezbaruah AN, Zhang TC. Fabrication of anodically electrodeposited iridium oxide film pH microelectrodes for microenviron-mental studies. Anal Chem. 2002. 10.1021/ac020326l.
55. Ges IA, Ivanov BL, Schaffer DK, Lima EA, Werdich AA, Baudenbacher FJ. Thin-film IrOx pH microelectrode for microfluidic-based microsystems. Biosens Bioelectron. 2005. 10.1016/j.bios.2004.09.021.
56. Cork SC, Eftekhar A, Mirza KB, Zuliani C, Nikolic K, Gardiner JV, Bloom SR, Toumazou C. Extracellular pH monitoring for use in closed-loop vagus nerve stimulation. J Neural Eng. 2018. 10.1088/1741-2552/aa8239.
57. Blau A, Ziegler C, Heyer M, Endres F, Schwitzgebel G, Matthies T, Stieglitz T, Meyer JU, Göpel W. Characterization and optimization of microelectrode arrays for in vivo nerve signal recording and stimulation. Biosens Bioelectron. 1997. 10.1016/S0956-5663(97)00017-1.
58. Weiland JD, Anderson DJ. Chronic neural stimulation with thin-film, iridium oxide electrodes. IEEE Trans Biomed Eng. 2000. 10.1109/10.846685.
59. Meyer RD, Cogan SF, Nguyen TH, Rauh RD. Electrodeposited iridium oxide for neural stimulation and recording electrodes. IEEE Trans Neural Syst Rehabil Eng. 2001. 10.1109/7333.918271.
60. Lee IS, Whang CN, Choi K, Choo MS, Lee YH. Characterization of iridium film as a stimulating neural electrode. Biomaterials. 2002. 10.1016/S0142-9612(01)00373-8.
61. Gawad S, Giugliano M, Heuschkel M, Wessling B, Markram H, Schnakenberg U, Renaud P, Morgan H. Substrate arrays of iridium oxide microelectrodes for in vitro neuronal interfacing. Front Neuroeng. 2009. 10.3389/neuro.16.001.2009.
62. Zhou H, Li T, Duan YY. Reduce impedance of intracortical iridium oxide microelectrodes by hydrogel coatings. Sensors Actuators, B Chem. 2012; 10.1016/j.snb.2011.10.019.
63. Rao L, Zhou H, Li T, Li C, Duan YY. Polyethylene glycol-containing polyurethane hydrogel coatings for improving the biocompatibility of neural electrodes. Acta Biomater. 2012. 10.1016/j.actbio.2012.03.001.
64. Fontes MBA. Electrodes for bio-application: recording and stimulation. J Phys Conf Ser. 2013. 10.1088/1742-6596/421/1/012019.

65. Kane SR, Cogan SF, Ehrlich J, Plante TD, McCreery DB, Troyk PR. Electrical performance of penetrating microelectrodes chronically implanted in cat cortex. IEEE Trans Biomed Eng. 2013. 10.1109/TBME.2013.2248152.
66. Yamagiwa S, Fujishiro A, Sawahata H, Numano R, Ishida M, Kawano T. Layer-by-layer assembled nanorough iridium-oxide/platinum-black for low-voltage microscale electrode neurostimulation. Sensors Actuators B Chem. 2015. 10.1016/j.snb.2014.09.048.
67. Yang H, Kang SK, Choi CA, Kim H, Shin DH, Kim YS, Kim YT. An iridium oxide reference electrode for use in microfabricated biosensors and biochips. Lab Chip. 2004. 10.1039/b309899k.
68. Franklin RK, Johnson MD, Scott KA, Shim JH, Nam H, Kipke DR, Brown RB. Iridium oxide reference electrodes for neurochemical sensing with MEMS microelectrode arrays. Proc IEEE Sensors. 2005. 10.1109/ICSENS.2005.1597971.
69. Ges IA, Ivanov BL, Werdich AA, Baudenbacher FJ. Differential pH measurements of metabolic cellular activity in nL culture volumes using microfabricated iridium oxide electrodes. Biosens Bioelectron. 2007. 10.1016/j.bios.2006.05.033.
70. Li C, Ahn CH, Shutter LA, Narayan RK. Toward real-time continuous brain glucose and oxygen monitoring with a smart catheter. Biosens Bioelectron. 2009. 10.1016/j.bios.2009.06.032.
71. Franklin RK, Joo S, Negi S, Solzbacher F, Brown RB. A comparison of fabrication methods for iridium oxide reference electrodes. Proc IEEE Sensors. 2009. 10.1109/ICSENS.2009.5398565.
72. Tolosa VM, Wassum KM, Maidment NT, Monbouquette HG. Electrochemically deposited iridium oxide reference electrode integrated with an electroenzymatic glutamate sensor on a multi-electrode array microprobe. Biosens Bioelectron. 2013. 10.1016/j.bios.2012.10.061.
73. Johnson MD, Kao OE, Kipke DR. Spatiotemporal pH dynamics following insertion of neural microelectrode arrays. J Neurosci Methods. 2007. 10.1016/j.jneumeth.2006.09.023.
74. Di Mario C, Grube E, Nisanci Y, Reifart N, Colombo A, Rodermann J, Muller R, Umman S, Liistro F, Montorfano M, Alt E. MOONLIGHT: a controlled registry of an iridium oxide-coated stent with angiographic follow-up. Int J Cardiol. 2004. 10.1016/j.ijcard.2003.10.007.
75. Pardue MT, Ball SL, Phillips MJ, Faulkner AE, Walker TA, Chow AY, Peachey NS. Status of the feline retina 5 years after subretinal implantation. J Rehabil Res Dev. 2006. 10.1682/JRRD.2005.07.0118.
76. Li M, Wang YB, Zhang X, Li QH, Liu Q, Cheng Y, Zheng YF, Xi TF, Wei SC. Surface characteristics and electrochemical corrosion behavior of NiTi alloy coated with IrO2. Mater Sci Eng C. 2013. 10.1016/j.msec.2012.07.026.
77. Chung T-W, Huang C-N, Chen P-C, Noda T, Tokuda T, Ohta J. Fabrication of iridium oxide/platinum composite film on titanium substrate for high-performance neurostimulation electrodes. Coatings. 2018. 10.3390/coatings8120420.
78. Chen C, Ruan S, Bai X, Lin C, Xie C, Lee IS. Patterned iridium oxide film as neural electrode interface: biocompatibility and improved neurite outgrowth with electrical stimulation. Mater Sci Eng C. 2019. 10.1016/j.msec.2019.109865.
79. Chung TW, Hsieh MT, Tso KC, Kuo SH, Cheng CT, Yu J, Chan TS, Wu PW, Chen PC. Synthesis and characterization of iridium oxide thin film via a pre-coordination step for bio-stimulating electrode application. Ceram Int. 2020. 10.1016/j.ceramint.2020.04.177.
80. Zhao ZH, Sakagami Y, Osaka T. Toxicity of hydrogen peroxide produced by electroplated coatings to pathogenic bacteria. Can J Microbiol. 1998. 10.1139/w98-030.
81. Stilling J, Ullah N, Omanovic S. Ir-Ni oxide as a promising material for nerve and brain stimulating electrodes. J Electrochem Sci Eng. 2014. 10.5599/jese.2014.0059.
82. Wessling B, Mokwa W, Schnakenberg U. RF-sputtering of iridium oxide to be used as stimulation material in functional medical implants. J Micromech Microeng. 2006. 10.1088/0960-1317/16/6/S21.
83. Kang X, Liu J, Tian H, Zhang C, Yang B, Nuli Y, Zhu H, Yang C. Controlled activation of iridium film for AIROF microelectrodes. Sensors Actuators B Chem. 2014. 10.1016/j.snb.2013.08.085.
84. Zeng Q, Xia K, Sun B, Yin Y, Wu T, Humayun MS. Electrodeposited iridium oxide on platinum nanocones for improving neural stimulation microelectrodes. Electrochim Acta. 2017. 10.1016/j.electacta.2017.03.213.

85. Ardizzone S, Carugati A, Trasatti S. Properties of thermally prepared iridium dioxide electrodes. J Electroanal Chem. 1981. 10.1016/S0022-0728(81)80437–8.

86. Schiavone LM, Dautremont-Smith WC, Beni G, Shay JL. Electrochromic iridium oxide films prepared by reactive sputtering. Appl Phys Lett. 1979. 10.1063/1.90950.

87. Kang X, Liu J, Tian H, Yang B, Nuli Y, Yang C. Optimization and electrochemical characterization of RF-sputtered iridium oxide microelectrodes for electrical stimulation. J Micromech Microeng. 2014. 10.1088/0960-1317/24/2/025015.

88. Robblee LS, Lefko JL, Brummer SB. Activated Ir: an electrode suitable for reversible charge injection in saline solution. J Electrochem Soc. 1983. 10.1149/1.2119793.

89. Yoshino T, Baba N, Arai K. Electrochromic IrOx thin films formed in sulfatoiridate (III, IV) complex solution by periodic reverse current electrolysis (PRIROF). Jpn J Appl Phys. 1987. 10.1143/JJAP.26.1547.

90. Rebec GV, Langley PE, Christopher Pierce R, Wang Z, Heidenreich BA. A simple micromanipulator for multiple uses in freely moving rats: electrophysiology, voltammetry, and simultaneous intracerebral infusions. J Neurosci Methods. 1993. 10.1016/0165-0270(93)90021-I.

91. Rebec GV, Christensen JRC, Guerra C, Bardo MT. Regional and temporal differences in real-time dopamine efflux in the nucleus accumbens during free-choice novelty. Brain Res. 1997. 10.1016/S0006-8993(97)01004-4.

92. Kiyatkin EA, Kiyatkin DE, Rebec GV. Phasic inhibition of dopamine uptake in nucleus accumbens induced by intravenous cocaine in freely behaving rats. Neuroscience. 2000. 10.1016/S0306-4522(00)00168-8.

93. Kishida KT, Sandberg SG, Lohrenz T, Comair YG, Sáez I, Phillips PEM, Montague PR. Sub-second dopamine detection in human striatum. PLoS One. 2011. 10.1371/journal.pone.0023291.

94. Kishida KT, Saez I, Lohrenz T, Witcher MR, Laxton AW, Tatter SB, White JP, Ellis TL, Phillips PEM, Montague PR. Subsecond dopamine fluctuations in human striatum encode superposed error signals about actual and counterfactual reward. Proc Natl Acad Sci U S A. 2016. 10.1073/pnas.1513619112.

95. Bennet KE, Tomshine JR, Min H-K, Manciu FS, Marsh MP, Paek SB, Settell ML, Nicolai EN, Blaha CD, Kouzani AZ, Chang S-Y, Lee KH. A diamond-based electrode for detection of neurochemicals in the human brain. Front Hum Neurosci. 2016. 10.3389/fnhum.2016.00102.

96. Moran RJ, Kishida KT, Lohrenz T, Saez I, Laxton AW, Witcher MR, Tatter SB, Ellis TL, Phillips PE, Dayan P, Montague PR. The protective action encoding of serotonin transients in the human brain. Neuropsychopharmacology. 2018. 10.1038/npp.2017.304.

97. Bang D, Kishida KT, Lohrenz T, White JP, Laxton AW, Tatter SB, Fleming SM, Montague PR. Sub-second dopamine and serotonin signaling in human striatum during perceptual decision-making. Neuron. 2020. 10.1016/j.neuron.2020.09.015.

98. Einaga Y Diamond electrodes for electrochemical analysis. J Appl Electrochem. 2010. 10.1007/s10800-010-0112-z.

99. Halpern JM, Xie S, Sutton GP, Higashikubo BT, Chestek CA, Lu H, Chiel HJ, Martin HB. Diamond electrodes for neurodynamic studies in Aplysia californica. Diam Relat Mater. 2006. 10.1016/j.diamond.2005.06.039.

100. Suzuki A, Ivandini TA, Yoshimi K, Fujishima A, Oyama G, Nakazato T, Hattori N, Kitazawa S, Einaga Y. Fabrication, characterization, and application of boron-doped diamond microelectrodes for in vivo dopamine detection. Anal Chem. 2007. 10.1021/ac071519h.

101. Yoshimi K, Naya Y, Mitani N, Kato T, Inoue M, Natori S, Takahashi T, Weitemier A, Nishikawa N, McHugh T, Einaga Y, Kitazawa S. Phasic reward responses in the monkey striatum as detected by voltammetry with diamond microelectrodes. Neurosci Res. 2011. 10.1016/j.neures.2011.05.013.

102. Fierro S, Yoshikawa M, Nagano O, Yoshimi K, Saya H, Einaga Y. In vivo assessment of cancerous tumors using boron doped diamond microelectrode. Sci Rep. 2012. 10.1038/srep00901.

103. Arumugam PU, Zeng H, Siddiqui S, Covey DP, Carlisle JA, Garris PA. Characterization of ultrananocrystalline diamond microsensors for in vivo dopamine detection. Appl Phys Lett. 2013. 10.1063/1.4811785.

104. Fierro S, Seishima R, Nagano O, Saya H, Einaga Y. In vivo pH monitoring using boron doped diamond microelectrode and silver needles: application to stomach disorder diagnosis. Sci Rep. 2013. 10.1038/srep03257.
105. Ogata G, Ishii Y, Asai K, Sano Y, Nin F, Yoshida T, Higuchi T, Sawamura S, Ota T, Hori K, Maeda K, Komune S, Doi K, Takai M, Findlay I, Kusuhara H, Einaga Y, Hibino H. A microsensing system for the in vivo real-time detection of local drug kinetics. Nat Biomed Eng. 2017. 10.1038/s41551-017-0118-5.
106. Ponnuswamy T, Chen JJ, Xu F, Chyan O. Monitoring metal ion contamination onset in hydrofluoric acid using silicon-diamond and dual silicon sensing electrode assembly. Analyst. 2001. 10.1039/b009841h.
107. Smirnov W, Yang N, Hoffmann R, Hees J, Obloh H, Müller-Sebert W, Nebel CE. Integrated all-diamond ultramicroelectrode arrays: optimization of faradaic and capacitive currents. Anal Chem. 2011. 10.1021/ac201595k.
108. Fan B, Zhu Y, Rechenberg R, Rusinek CA, Becker MF, Li W. Large-scale, all polycrystalline diamond structures transferred onto flexible Parylene-C films for neurotransmitter sensing. Lab Chip. 2017. 10.1039/c7lc00229g.
109. Ensch M, Maldonado VY, Swain GM, Rechenberg R, Becker MF, Schuelke T, Rusinek CA. Isatin detection using a boron-doped diamond 3-in-1 sensing platform. Anal Chem. 2018. 10.1021/acs.analchem.7b04045.
110. Fan B, Rusinek CA, Thompson CH, Setien M, Guo Y, Rechenberg R, Gong Y, Weber AJ, Becker MF, Purcell E, Li W. Flexible, diamond-based microelectrodes fabricated using the diamond growth side for neural sensing. Microsystems Nanoeng. 2020. 10.1038/s41378-020-0155-1.
111. Papo MJ, Catledge SA, Vohra YK, Machado C. Mechanical wear behavior of nanocrystalline and multilayer diamond coatings on temporomandibular joint implants. J Mater Sci Mater Med. 2004. 10.1023/B:JMSM.0000032817.05997.d2.
112. Bacakova L, Grausova L, Vacik J, Fraczek A, Blazewicz S, Kromka A, Vanecek M, Svorcik V. Improved adhesion and growth of human osteoblast-like MG 63 cells on biomaterials modified with carbon nanoparticles. Diam Relat Mater. 2007. 10.1016/j.diamond.2007.07.015.
113. Kalbacova M, Kalbac M, Dunsch L, Kromka A, Vaněček M, Rezek B, Hempel U, Kmoch S. The effect of SWCNT and nano-diamond films on human osteoblast cells. Phys Status Solidi. 2007. 10.1002/pssb.200776166.
114. Grausova L, Kromka A, Bacakova L, Potocky S, Vanecek M, Lisa V. Bone and vascular endothelial cells in cultures on nanocrystalline diamond films. Diam Relat Mater. 2008. 10.1016/j.diamond.2008.02.008.
115. Grausova L, Bacakova L, Kromka A, Vanecek M, Rezek B, Lisa V. Molecular markers of adhesion, maturation and immune activation of human osteoblast-like MG 63 cells on nanocrystalline diamond films. Diam Relat Mater. 2009. 10.1016/j.diamond.2008.10.023.
116. Kalbacova M, Rezek B, Baresova V, Wolf-Brandstetter C, Kromka A. Nanoscale topography of nanocrystalline diamonds promotes differentiation of osteoblasts. Acta Biomater. 2009. 10.1016/j.actbio.2009.04.020.
117. Grausova L, Bacakova L, Kromka A, Potocky S, Vanecek M, Nesladek M, Lisa V. Nanodiamond as promising material for bone tissue engineering. J Nanosci Nanotechnol. 2009. 10.1166/jnn.2009.NS26.
118. Rezek B, Ukraintsev E, Krátká M, Taylor A, Fendrych F, Mandys V. Epithelial cell morphology and adhesion on diamond films deposited and chemically modified by plasma processes. Biointerphases. 2014. 10.1116/1.4890471.
119. Suarez A, Prelas MA, Ghosh TK, Tompson RV, Loyalka SK, Miller WH, Viswanath DS. Diffusion of boron into polycrystalline diamond films using the electric field enhanced diffusion (EFED) technique. J Wide Bandgap Mater. 2002. 10.1177/1524511X02010001002.
120. Hasegawa R, Hirata-Koizumi M, Dourson ML, Parker A, Ono A, Hirose A. Safety assessment of boron by application of new uncertainty factors and their subdivision. Regul Toxicol Pharmacol. 2013. 10.1016/j.yrtph.2012.10.013.

121. Kromka A, Grausova L, Bacakova L, Vacik J, Rezek B, Vanecek M, Williams OA, Haenen K. Semiconducting to metallic-like boron doping of nanocrystalline diamond films and its effect on osteoblastic cells. Diam Relat Mater. 2010. 10.1016/j.diamond.2009.10.003.

122. Grausova L, Kromka A, Burdikova Z, Eckhardt A, Rezek B, Vacik J, Haenen K, Lisa V, Bacakova L. Enhanced growth and osteogenic differentiation of human osteoblast-like cells on boron-doped nanocrystalline diamond thin films. PLoS One. 2011. 10.1371/journal.pone.0020943.

123. Piret G, Hébert C, Mazellier JP, Rousseau L, Scorsone E, Cottance M, Lissorgues G, Heuschkel MO, Picaud S, Bergonzo P, Yvert B. 3D-nanostructured boron-doped diamond for microelectrode array neural interfacing. Biomaterials. 2015. 10.1016/j.biomaterials.2015.02.021.

124. Taylor AC, Vagaska B, Edgington R, Hébert C, Ferretti P, Bergonzo P, Jackman RB. Biocompatibility of nanostructured boron doped diamond for the attachment and proliferation of human neural stem cells. J Neural Eng. 2015. 10.1088/1741-2560/12/6/066016.

125. Garrett DJ, Saunders AL, McGowan C, Specks J, Ganesan K, Meffin H, Williams RA, Nayagam DAX. In vivo biocompatibility of boron doped and nitrogen included conductive-diamond for use in medical implants. J Biomed Mater Res Part B Appl Biomater. 2016. 10.1002/jbm.b.33331.

126. Alcaide M, Taylor A, Fjorback M, Zachar V, Pennisi CP. Boron-doped nanocrystalline diamond electrodes for neural interfaces: in vivo biocompatibility evaluation. Front Neurosci. 2016. 10.3389/fnins.2016.00087.

127. Torres-Martinez N, Cretallaz C, Ratel D, Mailley P, Gaude C, Costecalde T, Hebert C, Bergonzo P, Scorsone E, Mazellier JP, Divoux JL, Sauter-Starace F. Evaluation of chronically implanted subdural boron doped diamond/CNT recording electrodes in miniature swine brain. Bioelectrochemistry. 2019. 10.1016/j.bioelechem.2019.05.007.

128. Cobb SJ, Ayres ZJ, Macpherson JV. Boron doped diamond: a designer electrode material for the twenty-first century. Annu Rev Anal Chem. 2018. 10.1146/annurev-anchem-061417-010107.

129. Macpherson JV. A practical guide to using boron doped diamond in electrochemical research. Phys Chem Chem Phys. 2015. 10.1039/c4cp04022h.

130. Bergonzo P, Bongrain A, Scorsone E, Bendali A, Rousseau L, Lissorgues G, Mailley P, Li Y, Kauffmann T, Goy F, Yvert B, Sahel JA, Picaud S. 3D shaped mechanically flexible diamond microelectrode arrays for eye implant applications: the MEDINAS project. IRBM. 2011. 10.1016/j.irbm.2011.01.032.

131. Hess AE, Sabens DM, Martin HB, Zorman CA. Diamond-on-polymer microelectrode arrays fabricated using a chemical release transfer process. J Microelectromech Syst. 2011. 10.1109/JMEMS.2011.2159099.

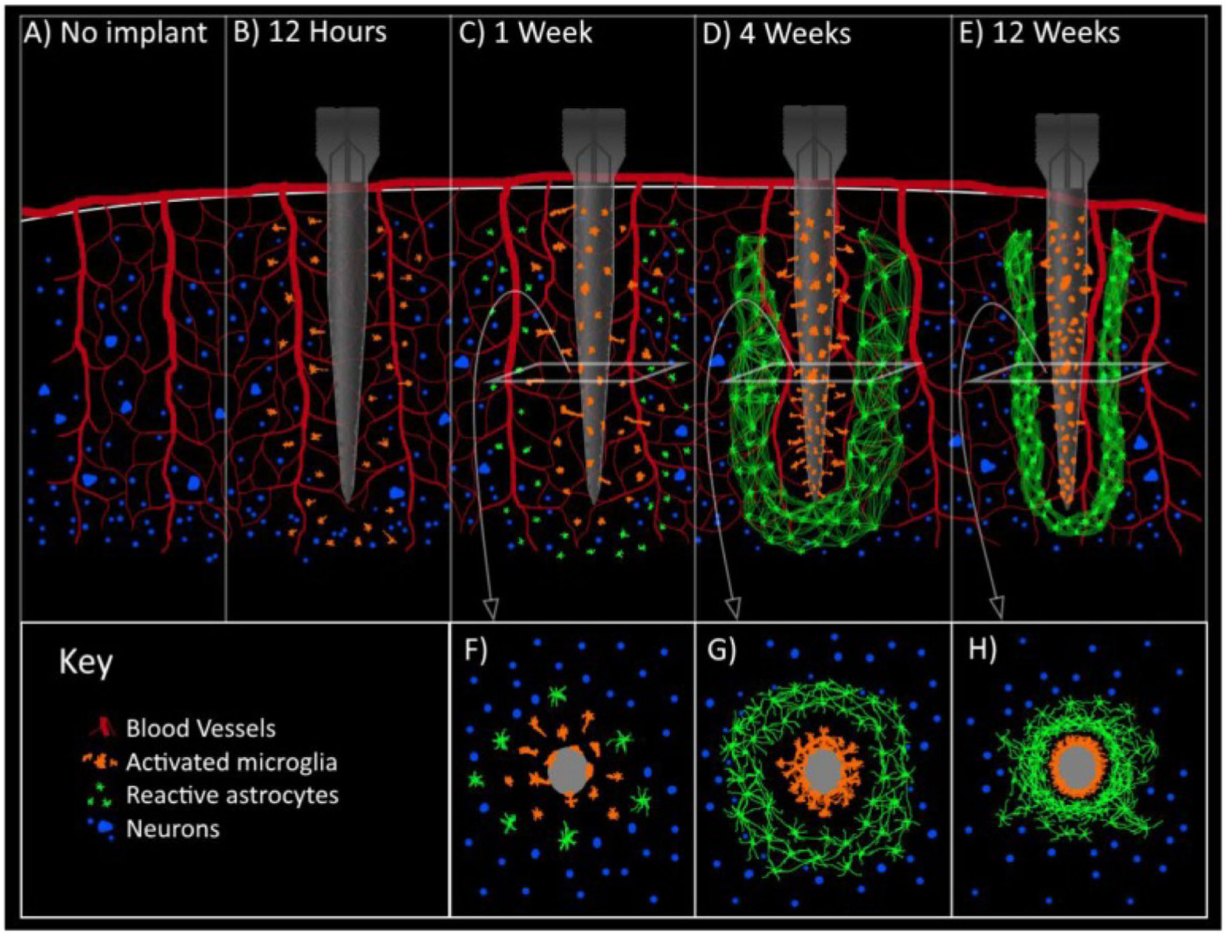

Fig. 1.

Electrode implantation in the brain elicits an immune response that leads to glial encapsulation of the electrode. Illustration of the immune response (**A**) prior to electrode implantation, (**B**) 12 h post-implantation—activated microglia migrate toward the electrode, (**C**) 1 week post-implantation—activated microglia have attached to the electrode and reactive astrocytes migrate toward the electrode, (**D**) 4 weeks post-implantation—the electrode is encapsulated by a sheath of activated microglia and reactive astrocytes, (**E**) 12 weeks post-implantation—the encapsulating glial sheath continues to tighten around the electrode. Cross-sectional views of (**C**), (**D**), and (**E**) are shown in (**F**), (**G**), and (**H**), respectively. Reproduced with permission from [19]

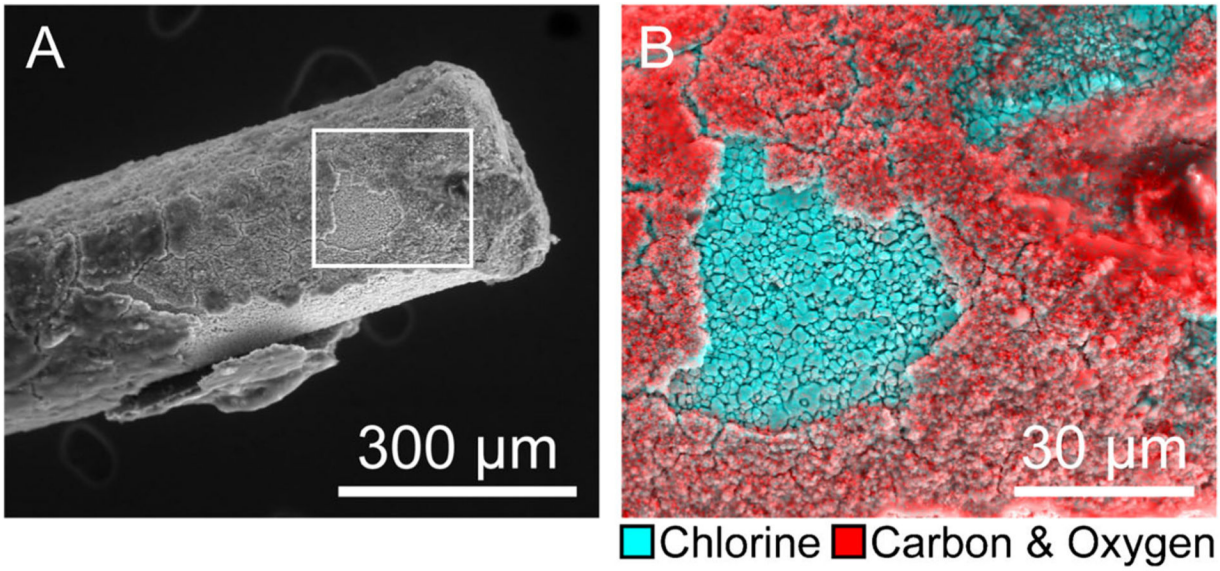

Fig. 2.

The encapsulation of chronically implanted Ag/AgCl reference electrodes diminishes surface chlorine. (**A**) 400× scanning electron micrograph of Ag/AgCl electrode, 3 weeks post-implantation. (**B**) 1500× box from **A**; EDX spectral mapping overlay: cyan = chlorine, red = carbon and oxygen. Reproduced with permission from [5].

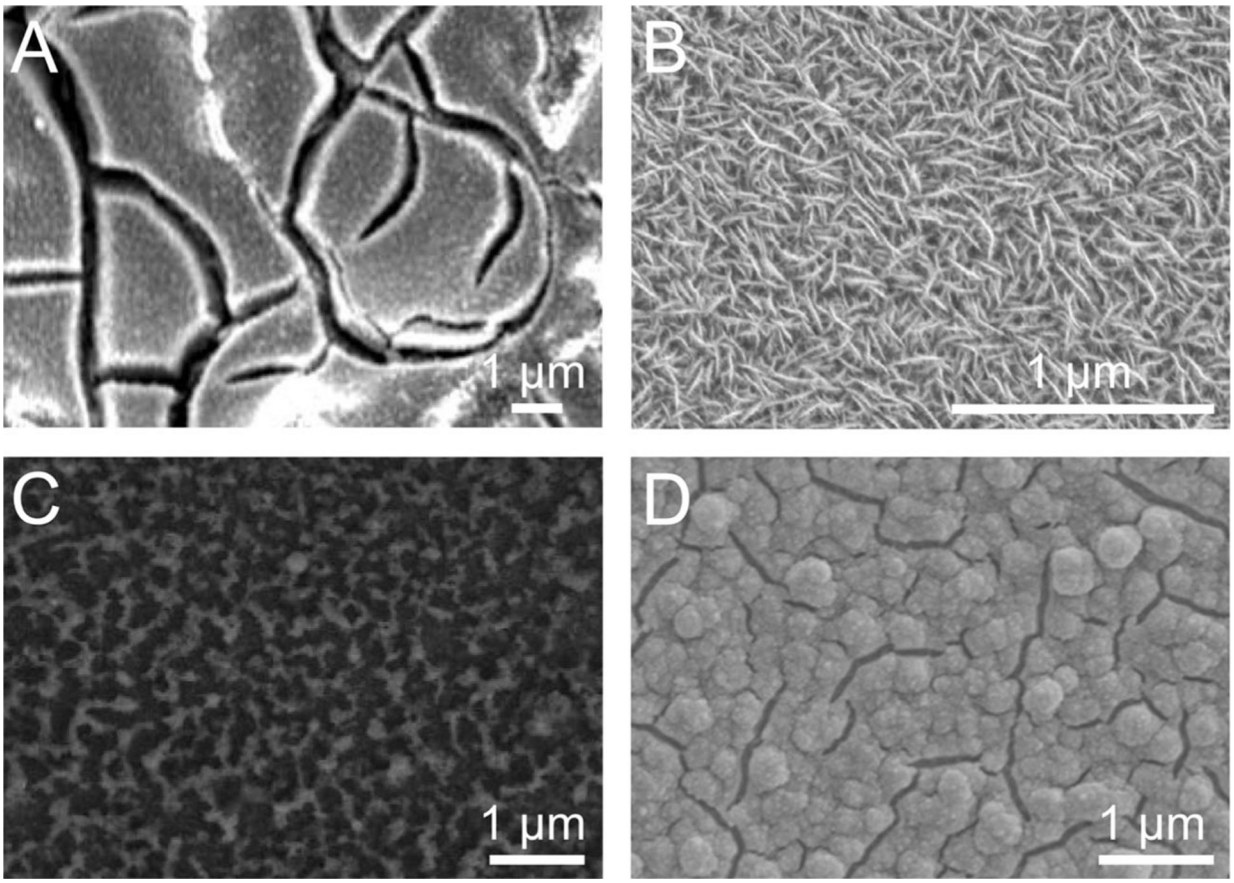

Fig. 3.

The surface morphology of an IrOx electrode is determined by the fabrication method and relevant parameters. Scanning electron micrographs of (**A**) thermal, (**B**) sputtered, (**C**) activated, and (**D**) electrodeposited IrOx films, adapted with permission from [81–84], respectively. Scale bars redrawn for consistency

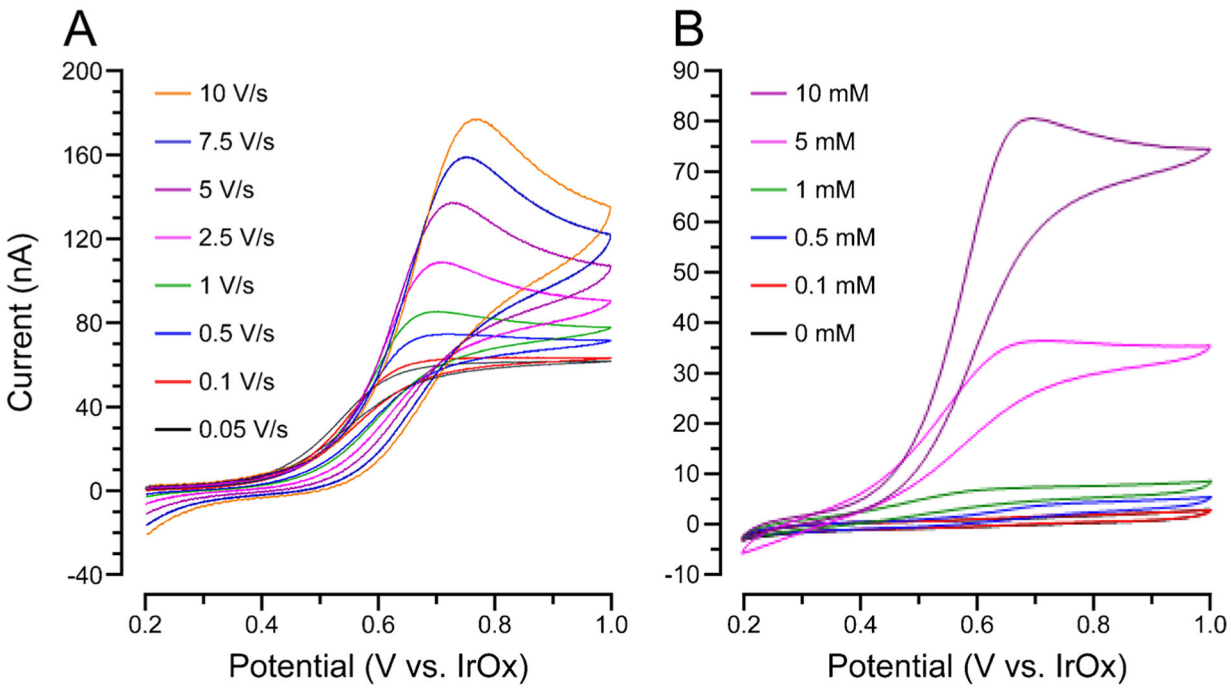

Fig. 4.

IrOx reference electrodes provide a stable potential for in vitro dopamine detection via cyclic voltammetry with Pt working and counter electrodes. Cyclic voltammetry of (**A**) 10 mM dopamine at various scan rates and (**B**) dopamine at various concentrations and a scan rate of 1 V/s. Adapted with permission from [71]. Axes and legends redrawn for clarity

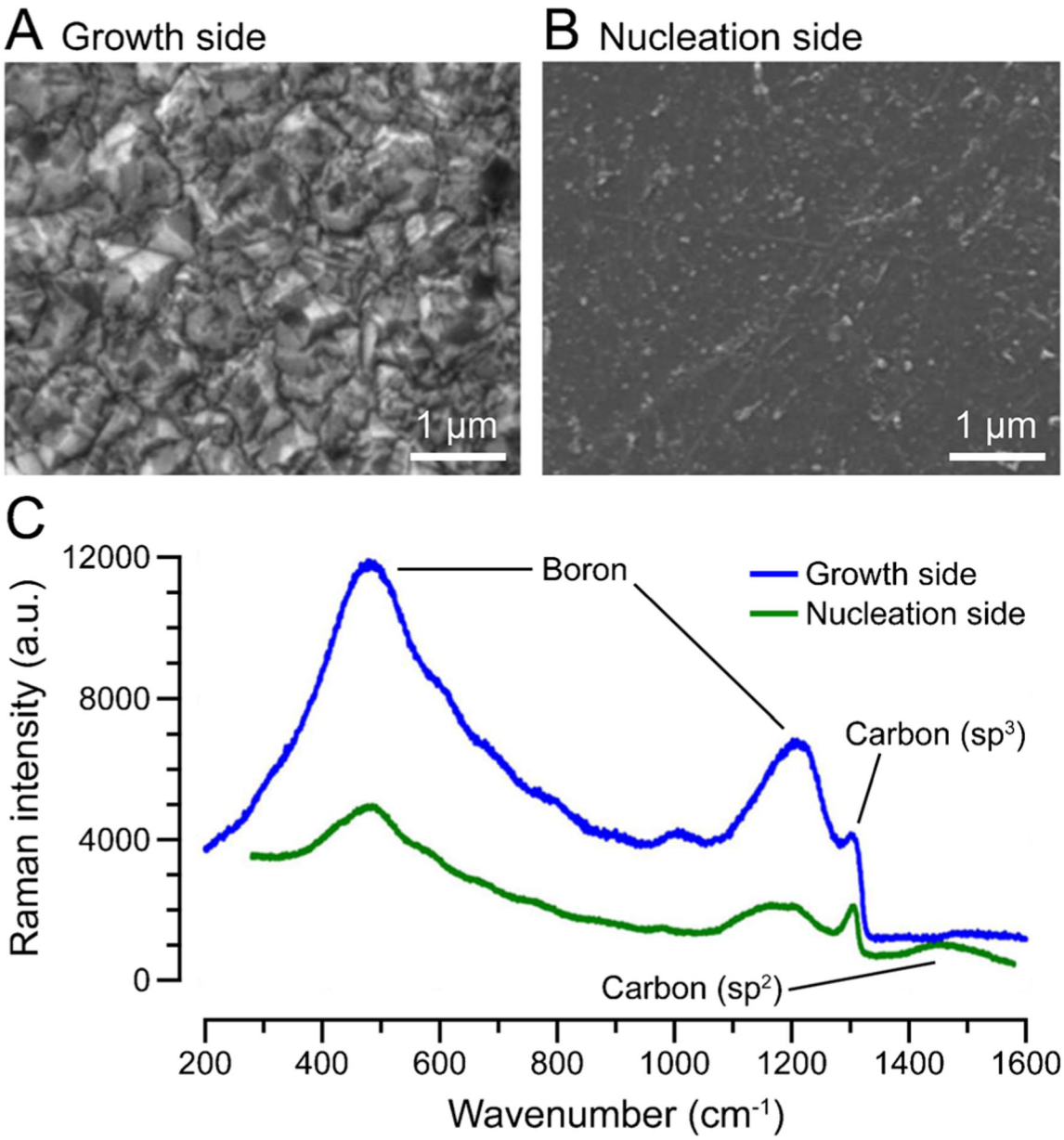

Fig. 5.

The BDD growth side exhibits favorable surface characteristics compared to the nucleation side. Scanning electron micrographs of (**A**) growth side and (**B**) nucleation side. (**C**) Raman spectrum of growth side (blue) and nucleation side (green). Adapted with permission from [110]. Scale bars, axes, and peak labels redrawn for clarity